Three-dimensional multi-target super-resolution microscopy of cells using Metal-Induced Energy Transfer and DNA-PAINT

Nazar Oleksiievets,[1,†] Nikolaos Mougios,[2, 3, †] Daniel C. Jans,[4, 5] Lara Hauke,[6,7] Jan Christoph Thiele,[8] Samrat Basak,[9] Stefan Jakobs,[4, 5, 10, 11] Felipe Opazo,[2, 12, 13] Jörg Enderlein,[9, 11, *] and Roman Tsukanov[9, *]

1. Max Planck Institute of Molecular Cell Biology and Genetics, 01307, Dresden.
2. Institute of Neuro-and Sensory Physiology, University Medical Center Göttingen, 37073 Göttingen, Germany.
3. International Max Planck Research School for Molecular Biology, 37077 Göttingen, Germany.
4. Department of NanoBiophotonics, Max Planck Institute for Multidisciplinary Sciences, 37077 Göttingen, Germany
5. Department of Neurology, University Medical Center Göttingen, 37073 Göttingen, Germany.
6. Institute of Pharmacology and Toxicology, University Medical Center,University of Göttingen, 37079 Göttingen, Germany.
7. CIDAS (Campus Institute Data Science), University of Göttingen, 37077 Göttingen, Germany.
8. Physical and Theoretical Chemistry Laboratory,Department of Chemistry, University of Oxford,South Parks Road, Oxford OX1 3QZ, U.K.
9. III. Institute of Physics – Biophysics, Georg August University, 37077 Göttingen, Germany.
10. Translational Neuroinflammation and Automated Microscopy, Fraunhofer Institute for Translational Medicine and Pharmacology ITMP, 37073 Göttingen, Germany.
11. Cluster of Excellence "Multiscale Bioimaging: from Molecular Machines to Networks of Excitable Cells" (MBExC),Georg August University, 37077 Göttingen, Germany.
12. Center for Biostructural Imaging of Neurodegeneration (BIN), University of Göttingen Medical Center, 37075 Göttingen, Germany.
13. NanoTag Biotechnologies GmbH, 37079 Göttingen, Germany.

† These authors contributed equally to this work.

* Corresponding authors: Jörg Enderlein jenderl@gwdg.de, Roman Tsukanov rtsukan@gwdg.de.

Keywords: super-resolution microscopy, DNA-PAINT, single-molecule localization microscopy, multiplexed imaging, fluorescence lifetime imaging microscopy, metal-induced energy transfer.

ABSRTACT

DNA-points accumulation for imaging in nanoscale topography (DNA-PAINT) is a potent variant of single-molecule localization microscopy (SMLM) which is highly effective for multiplexed super-resolution imaging. It achieves localization precision down to nanometers in the lateral direction. However, its routine axial localization precision is approximately three-fold lower as compared to the lateral localization precision. Recently, a technique known as Metal-Induced Energy Transfer (MIET) has been introduced, offering excellent axial resolution at the nanometer scale up to 200 nm above a surface. MIET is characterized by a low entry barrier, as its sole technical requirement is the availability of a fluorescence lifetime imaging modality. In this study, we harness the synergy between the exceptional axial resolution provided by MIET and the lateral resolution achieved with DNA-PAINT (MIET-PAINT) to accomplish multi-target 3D super-resolution imaging. We implemented MIET-PAINT using a wide-field fluorescence lifetime imaging microscope. We validated our technique by measuring the height of emitters placed on top of spacers of known thicknesses. We then demonstrated multiplexed MIET-PAINT imaging of fixed cells to visualize mechanotransduction proteins in the focal adhesion complex (FAC) and the cytoskeleton. We explored the structural arrangement of paxillin, zyxin, and actin stress fibers in U2OS cells and discovered that MIET-PAINT can reliably address multiple targets, providing lateral and axial nanometer-scale resolution.

INTRODUCTION

Multi-target bio-imaging offers an in-depth understanding of the structure and function of complex biological systems. For instance, it enables the mapping of intricate networks of intracellular interactions [1], or provides detailed insights into the organization of synapses [2], among other applications. Super-resolution microscopy (SRM) has become a cornerstone for biological investigations. The single-molecule localization microscopy (SMLM) suite of techniques, in particular, delivers superior resolution and can be easily adopted on most existing microscopes without the need for additional instrumentation. Prominent SMLM-based methods include photoactivatable localization microscopy (PALM) [3], stochastic optical reconstruction microscopy (STORM) [4], its more widely adopted variant direct STORM (dSTORM) [5], points accumulation for imaging in nanoscale topography (PAINT) [6], and DNA-PAINT [7, 8]. The latter technique, in particular, circumvents the significant limitation of fluorescence microscopy–the photobleaching of fluorophores–while taking advantage of the robustness, addressability, and designability of DNA molecules. In DNA-PAINT, targets are labeled by a docking single DNA strand identified by a complementary single strand DNA conjugated to a fluorophore termed "imager strand" freely diffusing in solution, ensuring continuous replenishment of fluorophores at labeling sites. The dwell time of a fluorophore at a target site is determined by the binding energy of the imager strand to its complementary strand. At the same time, the off-time primarily depends on the imager concentration, temperature, and salt concentration [7]. Additionally, multi-target (multiplexed) super-resolution imaging is readily achievable by labeling different targets with orthogonal DNA sequences. On the experimental front, numerous approaches exist for acquiring such multiplexed super-resolution data, with spectral splitting/demixing being among the most popular and widely utilized [9, 10]. Alongside rapid technological and instrumental developments, there has been significant progress in the development of probes for SRM [11].

Recent studies have shown that spectral splitting combined with fluorescence lifetime imaging microscopy (FLIM) can achieve highly multiplexed imaging [12]. dSTORM, when combined with spectral demixing, can facilitate up to three-color imaging [13, 14]. However, multiplexing capabilities of dSTORM are typically limited to three colors. This underscores the demand for a technique capable of highly multiplexed imaging with high resolution that is also easy to implement, preferably on standard scientific microscopes. DNA-PAINT addresses this challenge [7]: It is a powerful super-resolution technique, capable of imaging with nanometer localization precision and highly suitable for multi-target imaging [8]. In DNA-PAINT, multi-target imaging is achieved by using short labeled DNA strands (imagers) with orthogonal sequences that bind to complementary sequences (dockers) attached to targets of interest. Sequential imaging of targets can be realized through buffer exchange, a technique known as Exchange-PAINT [15]. However, the total acquisition time scales with the number of targets, making rapid multiplexed imaging, which can be achieved through parallel acquisition of targets by combining DNA-PAINT with spectral splitting [16] or by using tight control over DNA binding kinetics for kinetic barcoding [17], the ultimate goal. Despite the promise of DNA-PAINT using kinetic barcoding for cellular imaging, target identification and separation can become challenging due to significant crosstalk between targets, complicating target separation. In cellular DNA-PAINT imaging, the imager/docker binding kinetics is affected by the dense and sticky environment inside a cell. Fluorescence lifetime imaging microscopy (FLIM) provides fluorescence lifetime information as an addition to conventional intensity-based imaging. FLIM has found applications across a wide range of research fields, from material sciences to biology and medicine [18, 19]. A particularly attractive application of FLIM is in lifetime-based multiplexed imaging of cells, where lifetime information combined with spectral separation allows for the simultaneous imaging of multiple targets inside a cell [12, 20]. Recent advancements in FLIM detectors have facilitated the combination of FLIM with SMLM (Fluorescence Lifetime SMLM, or FL-SMLM) for both wide-field and confocal microscopy [21]. When DNA-PAINT data is acquired with lifetime information, it facilitates target identification and separation. This technique, named fluorescence lifetime DNA-PAINT (FL-PAINT), enables fast and parallel

acquisition of multiple targets [22]. FL-PAINT has been demonstrated using wide-field and confocal microscopy, with a comprehensive comparison of these two complementary FL-PAINT methods reported [23].

In the realm of SRM, achieving high axial resolution remains a challenge, with conventional techniques like DNA-PAINT offering nanometer-scale lateral resolution but lagging in axial precision by a factor of three or more [21]. While a few SRM methods such as supercritical angle fluorescence (SAF) [24], coherent fluorescence imaging with two objective lenses (4Pi detection) [25], 3D MINFLUX nanoscopy [26], 3D SMLM astigmatic imaging [27], and interferometric PALM [28] do offer higher axial resolution, they require complex setups and sophisticated data analysis, providing either tens of nanometers precision (astigmatism, biplane imaging) or nanometer precision with dedicated optical configurations.

The Metal-Induced Energy Transfer (MIET) technique, introduced ten years ago [29], promises nanometer axial localization precision and is straightforward to implement in optical setups equipped with fluorescence lifetime modality. MIET's efficiency hinges on the distance-dependent coupling of fluorescent dipole emission to surface plasmons in a metallic layer, typically gold, which can extend the technique's range to approximately 200 nm above the surface [30]. Additionally, covering the gold layer with a SiO_2 layer of designed thickness offers several advantages, including positioning objects of interest within MIET's most sensitive region, employing standard surface treatment protocols, and protecting the sensitive gold layer during immobilization procedures.

The distinctiveness of MIET lies in its extremely distance-dependent energy transfer efficiency, modulating an emitter's fluorescence lifetime and intensity to allow nanometer accurate distance measurements (single-molecule MIET or smMIET). This quenching effect, proportional to the distance to the surface, paradoxically increases the photo-stability of the emitter, ensuring a consistent number of photons emitted until photobleaching, largely independent of the dye-metal distance [31].

MIET has been successfully applied in a variety of biological studies, such as imaging blood platelet spreading and adhesion [32], actin cytoskeleton reorganization during epithelial-to-mesenchymal transformation [33], measuring nuclear envelope inter-bilayer distances [34], and elucidating the architecture of focal adhesions [35, 36]. Its capability extends to single-molecule applications as well [31, 37].

For applications requiring sub-nanometer axial precision, graphene-induced energy transfer (GIET) provides an attractive solution [38, 39], with a steep lifetime-distance dependency capable of resolving distances up to approximately 25 nm above the graphene surface [40, 41]. GIET's precision makes it particularly useful for studying membrane biophysics [42] and has been combined with DNA-PAINT for enhanced resolution imaging [41].

The integration of MIET's exceptional axial resolution with the lateral precision of SMLM techniques enables super-resolution imaging in 3D with nanometer range localization precision. A notable application is the combination of dSTORM with MIET, achieving simultaneous MIET-dSTORM imaging of dual targets through spectral splitting [43]. However, MIET-dSTORM faces limitations due to fluorophores photobleaching and the need for dyes with optimal blinking kinetics for concurrent imaging of various fluorophore types.

To address the challenges of multiplexing and imaging time, Exchange-PAINT [15, 44] offers a solution with its theoretically unlimited target imaging capacity, albeit with extended imaging times due to sequential imaging. An efficient strategy for rapid multiplexed imaging is the parallel acquisition of targets, exemplified by FL-PAINT, which significantly reduces total acquisition time [22].

In the current paper, we introduce MIET-PAINT, merging the high lateral localization precision and virtually unlimited multiplexing capacity of DNA-PAINT with MIET's exceptional axial localization precision. Implemented using a wide-field microscope equipped with a lifetime camera, MIET-PAINT employs microfluidics-assisted sequential imaging for highly multiplexed imaging. This innovative approach combines the strengths of both MIET and DNA-PAINT, offering an advanced toolkit for super-resolution biological imaging.

The focal adhesion complex (FAC) is a critical structure in cell-extracellular matrix (ECM) adhesion, facilitating force transduction, cytoskeletal regulation, and tension-dependent signaling [45]. FACs comprise hundreds of different proteins, organized in distinct layers and clusters, which play a pivotal role in mechano-sensing and force-transduction within a cell [46]. These complexes, extending approximately 200 nm above the substrate [46], have been the subject of extensive research, leading to detailed insights into protein localizations, binding partners, and associated pathways [47].

Near-field microscopy techniques such as SAF [24] and MIET imaging [29] are ideally suited for exploring the 3D architecture of focal adhesions. These methods have provided valuable perspectives on the maturation of nascent adhesions into FACs, the degradation of FACs, and the effects of various interventions [48]. We have previously utilized the nanometer-scaled axial resolution of MIET to study the three-dimensional organization of stress fibers and focal adhesions in fixed cells, focusing on actin and vinculin [35], and have demonstrated the feasibility of MIET imaging in live cells [49].

In this study, we introduce multi-target MIET-PAINT for 3D super-resolution imaging in fixed cells, specifically investigating the organization of FAC proteins and actin with nanometer localization precision. We targeted three proteins representing different layers of the adhesome: paxillin from the integrin-signaling layer at the base, zyxin from the actin regulatory layer at the top, and actin, a crucial component of the cytoskeleton involved in force transmission [46, 50]. These proteins were chosen for their roles in FAC formation and function, and their suitability for labeling and imaging with MIET-PAINT [51].

Paxillin, a key member of the integrin-signaling layer, is one of the first proteins recruited to nascent focal adhesions, facilitating the binding of other proteins and exhibiting force-dependent localization intensity within the FAC [48]. Labeling the phosphorylated subtype pPax-Y118, found exclusively in FAC clusters, allows us to explore its contribution to the dynamics of paxillin-FAK binding and thus to FAC stability and degradation [50, 52, 53]. Zyxin, a protein without specific subtypes limited to components of the force-transmission complex, is located both in the actin-regulatory FAC layer and along actin fibers, participating in the repair, stabilization, and thickening of actin stress fibers [48, 52, 54–56]. The recruitment and binding of zyxin are tension-dependent, with its incorporation into the FAC being stable and its attachment to stress fiber repair sites being transient [57]. By staining actin stress fibers, we can highlight a significant portion of the cell's force transduction mechanism [45, 50, 55]. Looking ahead, incorporating additional key FAC proteins such as FAK, VASP, and tubulin, will enable a more comprehensive understanding of force sensing, transmission, and generation within cells.

MIET-PAINT proves to be relatively straightforward to implement on a wide-field FLIM setup, offering precise lateral and nanometer-scale axial localization. The technique's strength lies in its capacity for 3D multi-target SRM imaging through sequential imaging of targets, showcasing its potential for detailed investigation of complex biological structures like the FAC.

RESULTS

Principle and validation of MIET-PAINT imaging

To verify the efficacy of the MIET-PAINT technique, we created a sample setup for imaging on top of SiO_2 layers of varying known thicknesses. This validation method, previously successful for calibrating MIET with stationary Atto 655 fluorophores [58], has now been adapted for MIET-PAINT by passivating the surface with docking strands, as illustrated in Figure 1a. We prepared gold slides with SiO_2 spacers of different thicknesses, achieving sub-nanometer precision in their preparation. Biotin-avidin chemistry was employed to specifically bind biotinylated docking strands to the SiO_2 surface, adding an additional ∼12 nm height from the biotin-avidin complex ("immobilization sandwich") to the fluorophores' absolute height above the gold layer [31].

During the experiments, imager strands were introduced into the chamber, and MIETPAINT imaging was conducted using our wide-field smFLIM optical setup, detailed in Figure S1 of the Supplementary Information (SI) and described in reference [58]. To expedite DNAPAINT acquisition, we utilized an optimized imager strand (R4-Atto 550), a development introduced by the Jungmann lab [59]. MIET-PAINT imaging was performed on SiO_2 spacers with thicknesses of 20, 30, 40, and 50 nm. Exemplary lifetime images are shown in Figure 1b, with the theoretical MIET curve used to convert lifetime values into heights depicted in Figure 1c, and an exemplary 3D MIET-PAINT image presented in Figure 1d. For each set of measurements, we generated a lifetime histogram and a corresponding height histogram, as displayed in Figure 1e-f. Upon comparing the experimentally measured heights with the designed height values, we observed complete agreement, as documented in Table S1 of the SI. It's important to note that, for accurate comparison between measured and designed heights, an additional ~12 nm must be considered to account for the thickness of the biotin-avidin immobilization layer. This comprehensive validation approach effectively demonstrates MIET-PAINT's precision and reliability for measuring fluorophore heights with nanometer accuracy within the sensitive MIET range of 100 nm above a surface.

Multi-target MIET-PAINT imaging of Focal Adhesion Complex

In this section, we showcase the application of multi-target MIET-PAINT imaging to cellular structures, focusing on proteins that play crucial roles in the formation of the Focal Adhesion Complex (FAC). By leveraging the sequential imaging capability of DNA-PAINT, akin to Exchange-PAINT [15], we label three targets with unique docking sequences. These docking strands are recognized by imager strands, all carrying the same fluorophore then completely avoiding the chromatic aberration. To enhance the speed and the efficiency of MIET-PAINT data acquisition, we utilized optimized imagers from the Jungmann lab [60], which improve the binding kinetics, thereby increasing the imager-docking binding rate. In MIET-PAINT imaging, this is particularly important to enhance the signal-to-background ratio, a critical factor for achieving high localization precision in MIET-PAINT imaging, as emitter fluorescence is quenched in the presence of a gold layer. We achieved this by reducing the background signal thanks to implementing concatenated docking strands [59]. Such docking strands are more efficient in capturing imager strand from a solution as compared to a conventional single-repeat docking strand. This allows to reduce imager concentration in a solution and therefore background signal while maintaining the same binding kinetics.

In MIET-PAINT imaging, enhancing the signal-to-background ratio is particularly crucial for achieving high localization precision. This factor becomes critical as emitter fluorescence is quenched in the presence of a gold layer. We accomplished this improvement by reducing the background signal through the implementation of concatenated docking strands [59]. These docking strands demonstrate greater efficiency in capturing imager strands from a solution compared to conventional single-repeat docking strands. This efficiency allows for a reduction in imager concentration in a solution, thereby minimizing background signal while maintaining consistent binding kinetics.

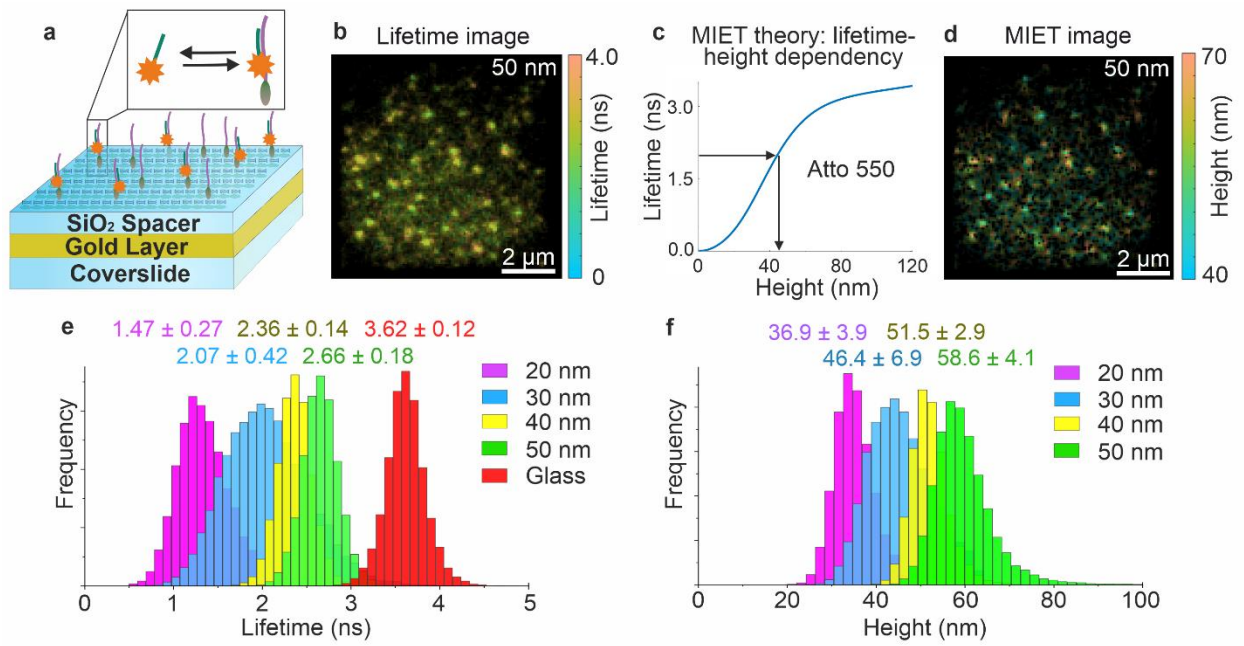

Figure 1. *The principle and validation of MIET-PAINT technique. (a) MIET-PAINT validation experiment design: gold glasses covered with SiO_2 spacers with different thicknesses are functionalized with docking strands via biotin-avidin chemistry; imager strand present in solution transiently binds to the complementary docking strand resulting in binding events. (b) Exemplary single-molecule MIET-PAINT lifetime image for 50 nm SiO_2 spacer (c) MIET theory: calculated lifetime-distance dependency for Atto 550 fluorophore attached to DNA. (d) Exemplary single-molecule MIET-PAINT height image obtained from (c). (e) Lifetime and (f) height histograms for different SiO_2 spacers thicknesses. The extra height of 12 nm is present in the experimental value due to the additional thickness of the immobilization layer. The average values and errors are displayed in colors that match those of the histograms.*

To further refine the localization accuracy of targeted, we minimized the linkage error-the distance between a reporter dye and the targeted object by labeling targets with single-domain antibodies (nanobodies). Nanobodies are markedly smaller than conventional antibodies, significantly reducing the spatial discrepancy between the position of a reporter dye and the tagged object [44].

Focusing on the architecture of FAC proteins, which are situated near the coverslip surface and within the sensitive MIET range of ~200 nm, allows for multiplexed MIET-PAINT imaging with high 3D localization precision. In analyzing MIET-PAINT data, we first localized binding events in the lateral direction, then determined emitter lifetimes from photon arrival times for each event, and finally applied the theoretical MIET lifetime-distance dependence to convert lifetime values into height measurements, thereby obtaining 3D localizations (see Methods section for detailed procedures).

Our investigation targeted two LIM-domain containing proteins, paxillin and zyxin [52, 55, 61, 62], and actin stress fibers [45], which are integral components of the cell's mechano-transduction machinery. Utilizing genome-edited homozygous Zyxin-rsEGFP2 U2OS cells in conjunction with commercially available anti-GFP nanobodies conjugated to DNA docking strands for zyxin labeling, anti-pPax-Y118 antibodies with anti-Rabbit secondary nanobodies for paxillin, and LifeAct for actin imaging [63], we selected cells for imaging based on the endogenous zyxin-EGFP2 signal, focusing on regions with mature FACs. The imaging process was sequentially executed for zyxin, paxillin pPax-Y118, and LifeAct, with each target imaged individually, followed by a comprehensive wash before the introduction of the next imager into the experimental chamber, as shown in Figure 2a-c and detailed in the Methods section.

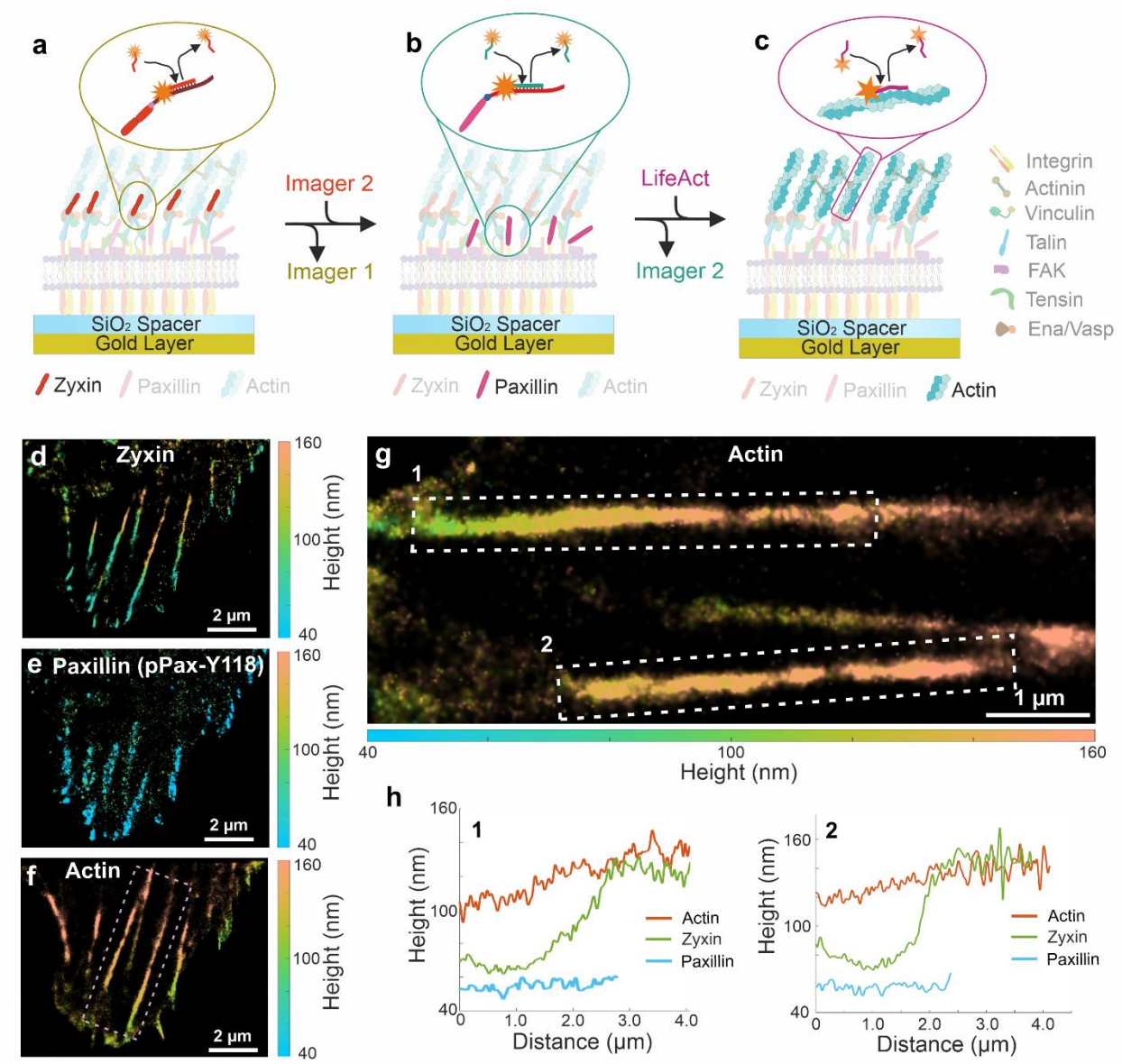

***Figure 2**. MIET-PAINT imaging of FAC and actin stress fibers. (a-c) Schematic of multi-target MIET-PAINT experiment demonstrated for the imaging of Focal Adhesion Complex proteins (zyxin and paxillin) and stress fibers. The targets are imaged sequentially, while each imaging cycle is performed with different imagers (or LifeAct in case of actin imaging). In between the imaging cycle, the previous imager is washed out and the next imager is introduced. MIET-PAINT images of zyxin (d), paxillin (pPax-Y118) (e), and actin (f) of the same cell. All scale bars are 2 µm. (g) Zoom-in region of actin image shown in (f). (h) Line height profiles of zyxin, paxillin, and actin along the stress fibers. The numbers depict the selection of two stress fibers as depicted in (g).*

We demonstrate MIET-PAINT imaging of zyxin, paxillin (pPax-Y118), and actin within the same cell, see Figure 2d-f and the original lifetime images in the Figure S4 in the SI. We further analyze the spatial arrangement of the selected targets by plotting the height profiles of each protein along stress fibers, see Figure 2g-h. MIET-PAINT images for another cell, the same targets are shown in Figure S5 in the SI. Our findings reveal that in the focal adhesion complex (FAC), phosphorylated paxillin clusters are located in a single layer at 52.7 ± 12.0 nm above the substrate, in full agreement with the previous reports. Zyxin is found in the actin regulatory layer of the FAC, located at a distance of ~60 nm above the substrate. Additionally, zyxin is colocalized with the LifeAct signal, indicating recruitment to stress fibers in a tension-

dependent manner. Actin stress fibers were observed at heights exceeding ~ 100 nm above the substrate and inclined at an average angle of 0.7°, in agreement with previous studies conducted on different cell types [29, 36]. We report average localization precisions of 22 nm lateral and 5 nm axial, as detailed in Table S3 in the SI.

Multi-target MIET-PAINT imaging allows for a comprehensive examination of the FAC, detailing the spatial organization and height variations of key proteins within the complex. Through strategic labeling and imaging, MIET-PAINT reveals the intricate 3D architecture of cellular structures involved in force transduction and adhesion, underlining the technique's potential for high-resolution, multiplexed imaging of biological systems.

DISCUSSION

Fluorescence lifetime adds significant value beyond what is achievable with conventional intensity-based super-resolution imaging. This additional lifetime information opens up diverse applications, such as rapid multiplexed imaging of multiple targets and environmental sensing. Specifically, we explore the utilization of lifetime data for precise axial localization of emitters through Metal-Induced Energy Transfer (MIET).

The integration of DNA-PAINT with MIET introduces a powerful method for achieving 3D super-resolution imaging, boasting localization precisions of less than 30 nm (30 nm lateral and 5 nm axial). DNA-PAINT provides an elegant solution to overcome the limitations of dye photobleaching, offering extensive flexibility in the choice of fluorophores for imaging. In MIET imaging, the ability to select fluorophores with optimal characteristics—such as high brightness, relatively long lifetime, and a narrow distribution of lifetimes—is essential for attaining high axial localization precision. The development of lifetime sensors for wide-field Fluorescence Lifetime Imaging Microscopy (FLIM) is advancing rapidly, promising the arrival of new-generation lifetime cameras with enhanced quantum efficiency (QE). Moreover, confocal-based FLIM presents a promising avenue for further enhancing MIET-PAINT imaging by optically reducing background noise, which significantly improves the signal-to-noise ratio. The QE of detectors typically used in confocal FLIM is significantly higher (over 50%), further contributing to the technique's effectiveness [23]. Highly multiplexed MIET-PAINT imaging becomes practical through sequential imaging of targets, akin to the Exchange-PAINT technique. By utilizing the same fluorophore across all targets, chromatic aberration is entirely eliminated. We showcased the potential of multitarget MIET-PAINT through imaging of FAC proteins, where the achieved resolution enables a comprehensive analysis of the architecture of FAC proteins. Specifically, we conducted MIET-PAINT imaging of paxillin (pPax-Y118), zyxin, and actin stress fibers. Our findings reveal that phosphorylated paxillin clusters are located in a single layer approximately 52.7 ± 12.0 nm above the substrate, aligning with prior studies [53, 64]. Zyxin was identified in the actin regulatory layer of the FAC, around 60 nm above the substrate, and was also found colocalized with LifeAct signals on stress fibers, where its recruitment is tension-dependent [52]. Actin stress fibers were observed at heights exceeding 100 nm above the substrate, inclining at an angle of 0.7°, consistent with findings from various cell types [29, 36].

In summary, MIET-PAINT emerges as a potent multi-target 3D super-resolution imaging technique, delivering high localization precision. It is applicable for imaging targets within close proximity to a coverslip surface (up to 200 nm) and can be relatively easily implemented on optical setups or microscopes equipped with a fluorescence lifetime modality. The DNA-PAINT methodology allows for the selection of fluorophores optimized for specific biological systems or microscope configurations, and for the adjustment of blinking kinetics to attain the highest localization precision.

METHODS

Calibration of MIET-PAINT

We designed an experiment for MIET-PAINT calibration as follows: the imager binding events were localized on top of SiO_2 spacers with different precisely determined thicknesses. Previously, such MIET validation strategy has proved to be successful for stationary Atto 655 fluorophores calibration [58]. For MIET-PAINT validation, we employed docking strand R4* [59], sequence (5'→3'): Biotin-ACACACACACACACACACA, for details see Table S2 in the SI. We used the docking strand R4* modified with biotin on its 5' end and immobilized it onto coverslip surface functionalized with BSA-biotin (A8549, Sigma-Aldrich) and then Neutravidin (31000, Thermo Fisher Scientific). We selected this docking strand as it has been used in the MIET-PAINT imaging of cells. The thickness of the biotin-avidin immobilization layer was reported to be ~12 nm [31], and was added to the spacer thickness to get total height value of an emitter above gold surface. The imager R4 had the following sequence (5'→3'): TGTGTGTTT and carried Atto 550 fluorophore on its 3' end. The imager was diluted to a concentration of ~0.5 nM in the imaging buffer PBS pH 7.4 with NaCl 500 mM and was injected into the Petri dish (Ibidi 81158, Germany). The imager-docker bindings events were detected and localized, while fluorescence lifetime for each event was extracted from TCSPC curves, see examples in Figure S3 in the SI. Then, the lifetime values were converted into axial positions, resulting in an emitter localization in 3D, see Table S1 in the SI. Series of measurements with different spacer thicknesses above gold layer has been performed using a wide-field FLIM setup, as shown in Figure S1 in the SI.

Cell culture

We used genome-edited U2OS cell line Zyxin-rsEGFP2 (homozygous), introduced previously in Ref [65]. The cells were cultivated in McCoys 5a medium (16600082, Thermo Fisher Scientific), supplemented with 100 U ml^{-1} penicillin, 100 ug ml^{-1} streptomycin (P0781, Sigma-Aldrich), 1 mM Na-pyruvate (S8636, Sigma-Aldrich) and 10% (v/v) FBS (FBS.S 0615, Bio and SELL) at 37°C, 5% CO_2.

Cell sample preparation

The cells were cultured for 1 day on 35 mm glass bottom (No. 1.5) dishes (81158, Ibidi), or, alternatively, in the same dishes but with gold coating. For the latter, following layers were used: 10 nm gold and 5 nm SiO_2. The cells were fixed in pre-warmed 8% formaldehyde in PBS for 10 min. After washing with PBS pH 7.4 the dish was stored at 4°C before
imaging.

Immunostaining of cells

Cells were permeabilized and blocked using 2% bovine serum albumin (BSA) and 0.2% Triton X-100 in PBS for 30 min at room temperature. PBS buffer containing nanobodies coupled to a docking strand (nanobodies concentration in range 20-50 nM) was used to stain the cells. The incubation time varied between 1-2h at room temperature. Finally, cells were washed three times for 15 minutes in total, rinsed with PBS buffer and then post-fixed with 4% PFA for 15 min at room temperature. The remaining aldehydes were quenched by 0.1 M glycine in PBS. Cells were stored in PBS at 4°C. The unconjugated nanobodies FluoTag-Q anti-GFP (NanoTag Biotechnologies GmbH, Germany, Cat. No: N0301) carrying one ectopic cysteine at the C-terminus allow for chemical couplings via a thiol-reactive compound. DNA docking strands (Biomers GmbH, Germany) were functionalized with an azide group at 5' end. The docking strands were coupled to the nanobodies using a dibenzocyclooctyne (DBCO) crosslinker [44]. FluoTag-Q anti-GFP was coupled to R4* concatenated sequence 5'-TACACACACACACACACACA-3' [59]. To label paxillin we employed the pre-mixing protocol [66]. Recombinant Anti-Paxillin (pPax-Y118) antibody (Abcam, ab32084, concentration 15 nM) and FluoTag-X2 anti-Rabbit IgG (NanoTag Biotechnologies

GmbH, N2402, Germany, the concentration of 45 nM) were pre-mixed in the tube and incubated for 30 minutes. FluoTag-X2 anti-Rabbit IgG was coupled to R1* docking sequence 5'-TCCTCCTCCTCCTCCTCCT-3' [59]. The fluorophore-labeled imager strands were purchased from Eurofins Genomics, Germany. The imagers were modified with Atto 550 fluorophore at its 3' end. The imagers were aliquoted in TE buffer (Tris 10mM, EDTA 1 mM, pH 8.0) at the concentration of 1 µM and stored at -20°C. Prior to the experiment, the strands were thawed and diluted to the final concentrations of 0.5 nM in PBS buffer pH 7.4 with 500 mM NaCl. Imager solution (~1 mL) was injected into a Petri dish with cells and MIET-PAINT imaging was performed. For actin imaging, we used commercially available LifeAct functionalized with Cy3B (Cambridge Research Biochemicals, crb1130929h, Billingham, UK). The original solution was diluted to a concentration of 1 µM, aliquoted and stored at -20°C. For imaging, we used LifeAct-Cy3B in a concentration of ~0.5 nM in PBS buffer pH 7.4 with 500 mM NaCl.

Data acquisition

Wide-field MIET-PAINT imaging of Zyxin cells

The experiments were performed using custom-built wide-field setup, see Figure S1 in the SI. The setup was equipped with a pulsed super-continuum white light laser (Fianium WhiteLase SC450, NKT Photonics) with pulse repetition of 20 MHz and a lifetime camera LINCam25 S20 (Photonscore GmbH) [67]. A custom-made photodiode (PD) was used to optically trigger the lifetime camera. TIR illumination mode was employed to achieve the best image contrast. Laser power after the optical fiber was ~10 mW. First, we used an emCCD camera to select a cell for MIET-PAINT imaging based on presence of focal adhesions in a cell, as detected by zyxin rsGFP signal. For the purpose, simultaneous illumination of 405 nm and 488 nm lasers was used: 405 nm for activation and 488 nm for excitation. Once a cell suitable for imaging was found, we switched acquisition to the lifetime camera and performed MIET-PAINT imaging. The targets were imaged in the following order: zyxin (discovered by imager R4-Atto 550), paxillin (pPax-Y118, discovered by imager R1-Atto 550) [59] and finally actin (discovered by LifeAct-Cy3B). The imagers were diluted to the concentration of ~0.5 nM in the imaging buffer (PBS-NaCl 500 mM) and were introduced into experimental chamber in a sequential manner (Exchange-PAINT). In between the imaging cycles the sample was washed with PBS until no localization events from a previous imaging round were detected. Then, next imager was introduced into the chamber. The lifetime data acquisition software was provided by Photonscore GmbH. A preliminary lifetime analysis was performed using the Photonscore Capture software. Typical acquisition time per target was 40 minutes.

Data analysis of MIET-PAINT experiment

For MIET-PAINT data analysis, we used previously published Matlab-based TrackNTrace analyse package [43] available online via link: https://github.com/scstein/TrackNTrace. In the current work, Matlab version R2022a was used for TrackNTrace data analysis. To obtain an emitter axial position, experimentally measured lifetime value of an emitter was converted into height using the theoretical MIET model [30]. Using literature values for refractive indices of gold and titanium literature [68] and given the sample geometry, lifetime-distance dependency (MIET curve) was calculated for the DNA-Atto 550 conjugate, as shown in Figure S2 in the SI. The following parameters were used for lifetime-distance dependency calculation (MIET curve): emission wavelength center 576 nm, quantum yield of 0.9, and free space lifetime of 3.74 ns. MIET curve for LifeAct-Cy3B was calculated using the following parameters: emission wavelength center 571 nm, quantum yield of 0.9, and free space lifetime of 2.7 ns. We assumed random orientation of emission dipole, as the C6 linker was used between a fluorophore and DNA. As the output format of the LINCam25 lifetime camera does not include division into pixels and time bin, therefore we were free to choose a spatial binning of 8 pixels, which corresponds to a virtual pixel size of 192 nm, and a time bin of 300 ms. The detection and precise sub-pixel localization of emitters was performed using a cross-correlation algorithm and pixel-integrated Gaussian MLE fitting. Non-repeating

localizations detected in a single frame were discarded. For each localization, lifetime information has been extracted by tail-fitting of a TCSPC curve with single-exponential function. For the purpose, TCSPC curve was cut 0.1 ns after the maximum, and the remaining decay was fitted with a mono-exponential function using a maximum likelihood estimator (MLE). A dataset was corrected for a lateral mechanical drift and, finally, a MIET-PAINT image was reconstructed. Following filters were applied to improve image quality: (1) localizations with more than 50 photons, (2) PSF sigma less than 1.8 px and (3) only lifetime values in the range from 0.5 ns to 5.0 ns were taken into account.

Corresponding authors

E-mail:(R.T.) rtsukan@gwdg.de. Phone: +49 551 39 26911. E-mail:(J.E.) jenderl@gwdg.de.
Phone: +49 551 39 26908.

ORCHID

J.C.T.: 0000-0002-6638-6298
L.H.: 0000-0003-0777-6859
N.M.: 0009-0007-5712-7175
R.T.: 0000-0002-3967-1755
D.C.J.: 0000-0002-6356-9742
J.E.: 0000-0001-5091-7157
S.B.: 0000-0002-1609-8642
F.O.: 0000-0002-4968-9713
S.J.: 0000-0002-8028-3121

Funding

J.E. acknowledges financial support from the DFG through Germany's Excellence Strategy EXC 2067/1–390729940. J.E. and S.B. are grateful to the European Research Council (ERC) via project "smMIET" (Grant agreement No. 884488) under the European Union's Horizon 2020 research and innovation program. N.M. and F.O. were supported by Deutsche Forschungsgemeinschaft (DFG) through the SFB 1286 (project Z04).

Notes

F.O. is a shareholder of NanoTag Biotechnologies GmbH. All other authors declare no competing interests.

Supplementary information

Wide-field FLIM optical setup for MIET-PAINT, Theoretical lifetime-height dependency - MIET curves, Buffer solutions, Validation of MIET-PAINT, Fluorescence lifetime decay curves, DNA sequences of imager and docker strands, Additional MIET-PAINT images, Quantitative characteristics of MIET-PAINT images.

Acknowledgment

The authors are grateful to Photonscore GmbH and personally to Yury Prokazov and André Weber for their support, valuable advice and contribution to the data analysis package. We thank Nicole Molitor for support with cell culture. We are grateful to Anna Chizhik for the preparation of gold-coated coverslips and Petri dishes. The authors thank Sebastian Isbaner for help during the initial stage of the project. We also thank Ingo Gregor for valuable advice.

Bibliography

[1] A. M. Valm, S. Cohen, W. R. Legant, J. Melunis, U. Hershberg, E. Wait, A. R. Cohen, M. W. Davidson, E. Betzig, and J. Lippincott-Schwartz, Applying systems-level spectral imaging and analysis to reveal the organelle interactome, Nature **546**, 162 (2017).

[2] B. G. Wilhelm, S. Mandad, S. Truckenbrodt, K. Kröhnert, C. Schäfer, B. Rammner, S. J. Koo, G. A. Claßen, M. Krauss, V. Haucke, H. Urlaub, and S. O. Rizzoli, Composition of isolated synaptic boutons reveals the amounts of vesicle trafficking proteins, Science **344**, 1023 (2014).

[3] [3] E. Betzig, G. H. Patterson, R. Sougrat, O. W. Lindwasser, S. Olenych, J. S. Bonifacino, M. W. Davidson, J. Lippincott-Schwartz, and H. F. Hess, Imaging intracellular fluorescent proteins at nanometer resolution, Science **313**, 1642 (2006).

[4] M. J. Rust, M. Bates, and X. Zhuang, Sub-diffraction-limit imaging by stochastic optical reconstruction microscopy (STORM), Nature Methods **3**, 793 (2006).

[5] S. Van de Linde, A. Löschberger, T. Klein, M. Heidbreder, S. Wolter, M. Heilemann, and M. Sauer, Direct stochastic optical reconstruction microscopy with standard fluorescent probes, Nat Protoc **6**, 991 (2011).

[6] A. Sharonov and R. M. Hochstrasser, Wide-field sub-diffraction imaging by accumulated binding of diffusing probes, Proc. Natl. Acad. Sci. **103**, 18911 (2006).

[7] R. Jungmann, C. Steinhauer, M. Scheible, A. Kuzyk, P. Tinnefeld, and F. C. Simmel, Single-molecule kinetics and super-resolution microscopy by fluorescence imaging of transient binding on DNA-Origami, Nano Letters **10**, 4756 (2010).

[8] J. Schnitzbauer, M. T. Strauss, T. Schlichthaerle, F. Schueder, and R. Jungmann, Super-resolution microscopy with DNA-PAINT, Nat. Protocols **12**, 1198 (2017).

[9] I. Testa, C. A. Wurm, R. Medda, E. Rothermel, C. von Middendorf, J. Fölling, S. Jakobs, A. Schönle, S. W. Hell, and C. Eggeling, Multicolor Fluorescence Nanoscopy in Fixed and Living Cells by Exciting Conventional Fluorophores with a Single Wavelength, Biophysical Journal **99**, 2686 (2010).

[10] K. Friedl, A. Mau, F. Boroni-Rueda, V. Caorsi, N. Bourg, S. Lévêque-Fort, and C. Leterrier, Assessing crosstalk in simultaneous multicolor single-molecule localization microscopy, Cell Reports Methods **0**, 10.1016/j.crmeth.2023.100571 (2023).

[11] E. D'Este, G. Lukinavičius, R. Lincoln, F. Opazo, and E. F. Fornasiero, Advancing cell biology with nanoscale fluorescence imaging: Essential practical considerations, Trends in Cell Biology 10.1016/j.tcb.2023.12.001 (2024).

[12] T. Niehörster, A. Löschberger, I. Gregor, B. Krämer, H.-J. Rahn, M. Patting, F. Koberling, J. Enderlein, and M. Sauer, Multi-target spectrally resolved fluorescence lifetime imaging microscopy, Nature Methods **13**, 257 (2016).

[13] A. Löschberger, S. van de Linde, M.-C. Dabauvalle, B. Rieger, M. Heilemann, G. Krohne, and M. Sauer, Super-resolution imaging visualizes the eightfold symmetry of gp210 proteins around the nuclear pore complex and resolves the central channel with nanometer resolution, Journal of Cell Science **125**, 570 (2012).

[14] Z. Zhang, S. J. Kenny, M. Hauser, W. Li, and K. Xu, Ultrahigh-throughput single-molecule spectroscopy and spectrally resolved super-resolution microscopy, Nature Methods **12**, 935 (2015).

[15] R. Jungmann, M. S. Avendano, M. Woehrstein, Johannes B. and Dai, W. M. Shih, and P. Yin, Multiplexed 3D cellular super-resolution imaging with DNA-PAINT and Exchange-PAINT, Nature Methods **11**, 313 (2014).

[16] N. Gimber, S. Strauss, R. Jungmann, and J. Schmoranzer, Simultaneous Multi-color DNA-PAINT without Sequential Fluid Exchange Using Spectral Demixing, Nano Letters 10.1021/acs.nanolett.1c04520 (2022).

[17] O. K. Wade, J. B. Woehrstein, P. C. Nickels, S. Strauss, F. Stehr, J. Stein, F. Schueder, M. T. Strauss, M. Ganji, J. Schnitzbauer, H. Grabmayr, P. Yin, P. Schwille, and R. Jungmann, 124-color super-resolution imaging by engineering DNA-PAINT blinking kinetics, Nano Letters **19**, 2641 (2019).

[18] M. Y. Berezin and S. Achilefu, Fluorescence Lifetime Measurements and Biological Imaging, Chemical reviews **110**, 2641 (2010).

[19] R. Datta, T. M. Heaster, J. T. Sharick, A. A. Gillette, and M. C. Skala, Fluorescence lifetime imaging microscopy: Fundamentals and advances in instrumentation, analysis, and applications, Journal of Biomedical Optics **25**, 071203 (2020).

[20] M. S. Frei, M. Tarnawski, M. J. Roberti, B. Koch, J. Hiblot, and K. Johnsson, Engineered Halo Tag variants for fluorescence lifetime multiplexing, Nature Methods **19**, 1 (2022).

[21] A. F. Koenderink, R. Tsukanov, J. Enderlein, I. Izeddin, and V. Krachmalnicoff, Super-resolution imaging: when biophysics meets nanophotonics, Nanophotonics **11**, 169 (2021).

[22] N. Oleksiievets, Y. Sargsyan, J. C. Thiele, N. Mougios, S. Sograte-Idrissi, O. Nevskyi, I. Gregor, F. Opazo, S. Thoms, J. Enderlein, and R. Tsukanov, Fluorescence lifetime DNA-PAINT for multiplexed super-resolution imaging of cells, Communications Biology **5**, 1 (2022).

[23] N. Oleksiievets, C. Mathew, J. C. Thiele, J. I. Gallea, O. Nevskyi, I. Gregor, A. Weber, R. Tsukanov, and J. Enderlein, Single-Molecule Fluorescence Lifetime Imaging Using Wide-Field and Confocal-Laser Scanning Microscopy: A Comparative Analysis, Nano Letters 10.1021/acs.nanolett.2c01586 (2022).

[24] C. Cabriel, N. Bourg, P. Jouchet, G. Dupuis, C. Leterrier, A. Baron, M.-A. Badet-Denisot, B. Vauzeilles, E. Fort, and S. Lévêque-Fort, Combining 3D single molecule localization strategies for reproducible bioimaging, Nature Communications **10**, 1980 (2019).

[25] M. Bates, J. Keller-Findeisen, A. Przybylski, A. Hüper, T. Stephan, P. Ilgen, A. R. Cereceda Delgado, E. D'Este, A. Egner, S. Jakobs, S. J. Sahl, and S. W. Hell, Optimal precision and accuracy in 4Pi-STORM using dynamic spline PSF models, Nature Methods **19**, 603 (2022).

[26] K. C. Gwosch, J. K. Pape, F. Balzarotti, P. Hoess, J. Ellenberg, J. Ries, and S. W. Hell, MINFLUX nanoscopy delivers 3D multi-color nanometer resolution in cells, Nature Methods **17**, 217 (2020).

[27] B. Huang, W. Wang, M. Bates, and X. Zhuang, Three-Dimensional Super-Resolution Imaging by Stochastic Optical Reconstruction Microscopy, Science **319**, 810 (2008).

[28] G. Shtengel, J. A. Galbraith, C. G. Galbraith, J. Lippincott-Schwartz, J. M. Gillette, S. Manley, R. Sougrat, C. M. Waterman, P. Kanchanawong, M. W. Davidson, R. D. Fetter, and H. F. Hess,

Interferometric fluorescent super-resolution microscopy resolves 3D cellular ultrastructure, Proceedings of the National Academy of Sciences **106**, 3125 (2009).

[29] A. I. Chizhik, J. Rother, I. Gregor, A. Janshoff, and J. Enderlein, Metal-induced energy transfer for live cell nanoscopy, Nature Photonics **8**, 124 (2014).

[30] J. Enderlein, Single-molecule fluorescence near a metal layer, Chemical Physics **247**, 1 (1999).

[31] S. Isbaner, N. Karedla, I. Kaminska, D. Ruhlandt, M. Raab, J. Bohlen, A. Chizhik, I. Gregor, P. Tinnefeld, J. Enderlein, *et al.*, Axial colocalization of single molecules with nanometer accuracy using metal-induced energy transfer, Nano letters **18**, 2616 (2018).

[32] A. Zelena, S. Isbaner, D. Ruhlandt, A. Chizhik, C. Cassini, A. S. Klymchenko, J. Enderlein, A. Chizhik, and S. Köster, Time-resolved MIET measurements of blood platelet spreading and adhesion, Nanoscale **12**, 21306 (2020).

[33] T. Baronsky, D. Ruhlandt, B. R. Brückner, J. Schäfer, N. Karedla, S. Isbaner, D. Hähnel, I. Gregor, J. Enderlein, A. Janshoff, and A. I. Chizhik, Cell–Substrate Dynamics of the Epithelial-to-Mesenchymal Transition, Nano Letters **17**, 3320 (2017).

[34] A. M. Chizhik, D. Ruhlandt, J. Pfaff, N. Karedla, A. I. Chizhik, I. Gregor, R. H. Kehlenbach, and J. Enderlein, Three-Dimensional Reconstruction of Nuclear Envelope Architecture Using Dual-Color Metal-Induced Energy Transfer Imaging, ACS Nano **11**, 11839 (2017).

[35] A. M. Chizhik, C. Wollnik, D. Ruhlandt, N. Karedla, A. I. Chizhik, L. Hauke, D. Hähnel, I. Gregor, J. Enderlein, and F. Rehfeldt, Dual-color metal-induced and Förster resonance energy transfer for cell nanoscopy, Molecular Biology of the Cell **29**, 846 (2018).

[36] C. Grandy, F. Port, J. Pfeil, and K.-E. Gottschalk, Influence of ROCK Pathway Manipulation on the Actin Cytoskeleton Height, Cells **11**, 430 (2022).

[37] N. Karedla, A. I. Chizhik, I. Gregor, A. M. Chizhik, O. Schulz, and J. Enderlein, Single-molecule metal-induced energy transfer (smMIET): Resolving nanometer distances at the single-molecule level, ChemPhysChem **15**, 705 (2014).

[38] A. Ghosh, A. Sharma, A. I. Chizhik, S. Isbaner, D. Ruhlandt, R. Tsukanov, I. Gregor, N. Karedla, and J. Enderlein, Graphene-based metal-induced energy transfer for sub-nanometre optical localization, Nature Photonics **13**, 860 (2019).

[39] I. Kaminska, J. Bohlen, S. Rocchetti, F. Selbach, G. P. Acuna, and P. Tinnefeld, Distance Dependence of Single-Molecule Energy Transfer to Graphene Measured with DNA Origami Nanopositioners, Nano Letters **19**, 4257 (2019).

[40] A. Ghosh, A. I. Chizhik, N. Karedla, and J. Enderlein, Graphene- and metal-induced energy transfer for single-molecule imaging and live-cell nanoscopy with (sub)-nanometer axial resolution, Nature Protocols **16**, 3695 (2021).

[41] I. Kaminska, J. Bohlen, R. Yaadav, P. Schüler, M. Raab, T. Schröder, J. Zähringer, K. Zielonka, S. Krause, and P. Tinnefeld, Graphene Energy Transfer for Single-Molecule Biophysics, Biosensing, and Super-Resolution Microscopy, Advanced Materials **33**, 2101099 (2021).

[42] T. Chen, A. Ghosh, and J. Enderlein, Cholesterol-Induced Nanoscale Variations in the Thickness of Phospholipid Membranes, Nano Letters **23**, 2421 (2023).

[43] J. C. Thiele, M. Jungblut, D. A. Helmerich, R. Tsukanov, A. Chizhik, A. I. Chizhik, M. J. Schnermann, M. Sauer, O. Nevskyi, and J. Enderlein, Isotropic three-dimensional dual-color super-resolution microscopy with metal-induced energy transfer, Science Advances **8**, 2506 (2022).

[44] S. Sograte-Idrissi, N. Oleksiievets, S. Isbaner, M. Eggert-Martinez, J. Enderlein, R. Tsukanov, and F. Opazo, Nanobody detection of standard fluorescent proteins enables multi-target DNA-PAINT with high resolution and minimal displacement errors, Cells **8**, 48 (2019).

[45] Z. Sun, S. S. Guo, and R. Fässler, Integrin-mediated mechanotransduction, Journal of Cell Biology **215**, 10.1083/jcb.201609037 (2016).

[46] P. Kanachanawong, G. Shtengel, A. M. Pasapera, E. B. Ramko, M. W. Davidson, H. F. Hess, and C. M. Waterman, Nanoscale architecture of integrin-based cell adhesions, Nature **468**, 10.1038/nature09621 (2010).

[47] K. N. Murphy and A. J. Brinkworth, Manipulation of focal adhesion signaling by pathogenic microbes, International Journal of Molecular Sciences **22**, 10.3390/ijms2203135 (2021).

[48] K. Legerstee, B. Geverts, J. A. Slotman, and A. B. Houtsmuller, Dynamics and distribution of paxillin, vinculin, zyxin and vasp depend on focal adhesion location and orientation, Scientific Reports **9**, 10.1038/s41598-019-46905-2 (2019).

[49] L. Hauke, S. Isbaner, A. Ghosh, I. Guido, L. Turco, A. I. Chizhik, I. Gregor, N. Karedla, F. Rehfeldt, and J. Enderlein, Metal-Induced Energy Transfer (MIET) for Live-Cell Imaging with Fluorescent Proteins, ACS Nano 10.1021/acsnano.2c12372 (2023).

[50] M. Ripamonti, B. Wehrle-Haller, and I. de Curtis, Paxillin: A hub for mechano-transduction from the β3 integrin-talin-kindlin axis, Frontiers in Cell and Developmental Biology **10**, 10.3389/fcell.2022.852016 (2022).

[51] M. Bachmann, A. Skripka, K. Weißenbruch, B. Wehrle-Haller, and M. Bastmeyer, Phosphorylated paxillin and phosphorylated fak constitute subregions within focal adhesions, Journal of Cell Science **135**, 10.1242/jcs.258764 (2022).

[52] M. A. Smith, E. Blankmann, N. O. Deakin, L. M. Hoffmann, C. C. Jensen, C. E. Turner, and M. C. Beckerle, Lim domains target actin regulators paxillin and zyxin to sites of stress fiber strain, PLoS ONE **8**, 10.1371/journal.pone.0069378 (2013).

[53] R. Zaidel-Bar, R. Milo, Z. Kam, and B. Geiger, A paxillin tyrosine phosphorylation switch regulates the assembly and form of cell-matrix adhesions, Journal of Cell Science **120**, 10.1242/jcs.03314 (2007).

[54] J. Colombelli, A. Besser, H. Kress, E. G. Reynaud, P. Girard, E. Caussinus, U. Haselmann, J. V. Small, U. S. Schwarz, and E. H. K. Stelzer, Mechanosensing in actin stress fibers revealed by a close correlation between force and protein localization, Journal of Cell Science **122**, 10.1242/jcs.042986 (2009).

[55] L. M. Hoffmann, C. C. Jensen, A. Chaturvedi, M. Yoshigi, and M. C. Beckerle, Stretch induced actin remodeling requires targeting of zyxin to stress fibers and recruitment of actin regulators, Molecular Biology of the Cell **23**, 10.1091/mbc.E11-12-1057 (2012).

[56] M. Yoshigi, L. M. Hoffman, c. C. Jensen, J. Yost, and M. C. Beckerle, Mechanical force mobilizes zyxin from focal adhesions to actin filaments and regulates cytoskeletal reinforcement, Journal of Cell Biology **171**, 10.1083/jcb.200505018 (2005).

[57] M. A. Smith, E. Blankmann, M. L. Gardel, L. Luetthohann, C. W. Waterman, and M. C. Beckerle, A zyxin-mediated mechanism for actin stress fiber maintenance and repair, Developmental Cell **19**, 10.1016/j.devcel.2010.08.008 (2010).

[58] N. Oleksiievets, J. C. Thiele, A. Weber, I. Gregor, O. Nevskyi, S. Isbaner, R. Tsukanov, and J. Enderlein, Wide-field fluorescence lifetime imaging of single molecules, The Journal of Physical Chemistry A **124**, 3494 (2020).

[59] S. Strauss and R. Jungmann, Up to 100-fold speed-up and multiplexing in optimized DNA-PAINT, Nature Methods **17**, 789 (2020).

[60] F. Schueder, J. Stein, F. Stehr, A. Auer, B. Sperl, M. T. Strauss, P. Schwille, and R. Jungmann, An order of magnitude faster dna-paint imaging by optimized sequence design and buffer conditions, Nature Methods **16**, 1101 (2019).

[61] R. Yan, X. Ge, N. Pang, H. Ye, L. Yuan, B. Cheng, K. Zhou, M. Yang, Y. Sun, S. Zhang, Z. Ding, J. Luo, C. Ruan, and K. Dai, Essential role of zyxin in platelet biogenesis and glycoprotein Ib-IX surface expression, Cell Death & Disease **12**, 1 (2021).

[62] A. J. Woods, M. S. Roberts, J. Choudhary, S. T. Barry, Y. Mazaki, H. Sabe, S. J. Morley, D. R. Critchley, and J. C. Norman, Paxillin Associates with Poly(A)-binding Protein 1 at the Dense Endoplasmic Reticulum and the Leading Edge of Migrating Cells*, Journal of Biological Chemistry **277**, 6428 (2002).

[63] J. Riedl, A. H. Crevenna, K. Kessenbrock, J. H. Yu, D. Neukirchen, M. Bista, F. Bradke, D. Jenne, T. A. Holak, Z. Werb, M. Sixt, and R. Wedlich-Soldner, Lifeact: A versatile marker to visualize F-actin, Nature methods **5**, 605 (2008).

[64] P. Kanchanawong, G. Shtengel, A. M. Pasapera, E. B. Ramko, M. W. Davidson, H. F. Hess, and C. M. Waterman, Nanoscale architecture of integrin-based cell adhesions, Nature **468**, 580 (2010).

[65] M. Ratz, I. Testa, S. W. Hell, and S. Jakobs, CRISPR/Cas9-mediated endogenous protein tagging for RESOLFT super-resolution microscopy of living human cells, Scientific Reports **5**, 9592 (2015).

[66] S. Sograte-Idrissi, T. Schlichthaerle, C. J. Duque-Afonso, M. Alevra, S. Strauss, T. Moser, R. Jungmann, S. O. Rizzoli, and F. Opazo, Circumvention of common labelling artefacts using secondary nanobodies, Nanoscale **12**, 10226 (2020).

[67] Y. Prokazov, E. Turbin, A. Weber, R. Hartig, and W. Zuschratter, Position sensitive detector for fluorescence lifetime imaging, Journal of Instrumentation **9** (12), C12015.

[68] A. D. Rakic, A. B. Djurisic, J. M. Elazar, and M. L. Majewski, Optical properties of metallic films for vertical-cavity optoelectronic devices, Appl. Opt. **37**, 5271 (1998).